J|A|C|S
ARTICLES
Published on Web 05/18/2007

Tuning of Redox Properties of Iron and Iron Oxides via Encapsulation within Carbon Nanotubes

Wei Chen, Xiulian Pan, and Xinhe Bao*

Contribution from the State Key Laboratory of Catalysis, Dalian Institute of Chemical Physics, Chinese Academy of Sciences, Zhongshan Road 457, Dalian 116023, P. R. China

Received February 23, 2007; E-mail: xhbao@dicp.ac.cn

Abstract: We report the tuning of the redox properties of iron and iron oxide nanoparticles by encapsulation within carbon nanotubes (CNTs) with varying inner diameters. Raman spectroscopy was employed to investigate the interaction of the encapsulated nanoparticles with the CNTs. A red shift of the Fe−O mode is observed in the nanoparticles deposited on the outer CNT surfaces with respect to bulk Fe_2O_3. However, this mode is found to be stepwise blue-shifted with decreasing inner diameter in the CNT-encapsulated Fe_2O_3 nanoparticles, suggesting an enhanced interaction of Fe_2O_3 with the inner CNT surface as its curvature increases. The autoreduction of the encapsulated Fe_2O_3 is significantly facilitated inside CNTs with respect to the outside nanoparticles. Interestingly, it becomes more facile with decreasing CNT channel diameter as evidenced by temperature programmed reaction, in situ XRD, and Raman spectroscopy. The oxidation of encapsulated metallic Fe nanoparticles on the other hand is retarded in comparison to that of the outside Fe particles as shown by in situ XRD and gravimetrical measurements with an online microbalance. We attribute this tunable redox behavior of transition metal nanoparticles inside CNTs to a particular electronic interaction of the encapsulates with the interior CNT surface, which stabilizes the metallic state of Fe.

1. Introduction

Carbon nanotubes (CNTs) exhibit a well-defined tubular morphology and are proposed to be utilized as templates for the synthesis of other nanomaterials or as nanosized reaction vessels.[1−3] Theoretical studies indicate that chemical reactions could be sensitive to the confinement in nanoscopic channels of CNTs.[2−3] The nonplanar sp^2-hybridized carbon framework and properties such as good electrical conductivity, mechanical strength, and thermal stability[4] also make CNTs intriguing catalyst supports. Many studies have shown the benefits of using CNTs as supports to disperse transition metal catalysts on the outer CNT surface for liquid-phase hydrogenation and fuel cell electrode reactions resulting in an improved activity and/or product selectivity.[5−8] However, few efforts have been made to carry out reactions on transition metal catalysts encapsulated within nanotubes,[9−10] although this may bring forth an unexpected and interesting catalytic performance due to the combination of the unique properties of nanotubes and the confinement effect of the channels.

Although extensive studies have been undertaken to introduce transition metals into the CNT channels,[11−13] there is a lack of knowledge of the physiochemical properties of encapsulated transition metal nanoparticles. In particular the redox behavior and chemical stability of the encapsulated transition metals are essential for applications in catalysis. Iron, a typical d-block transition metal, and its oxides are important catalysts for many reactions, e.g., Fischer−Tropsch, ammonia synthesis,[14] or ethylbenzene dehydrogenation to styrene.[15] We have previously found that CNT-confined Fe_2O_3 nanoparticles can be autoreduced and that this process is facilitated when they are located inside CNT channels rather than on the outer surface of CNTs.[16] Here we study systematically the redox behavior of the encapsulated Fe and Fe_2O_3 nanoparticles. The results obtained from a series of in situ characterization experiments such as temperature programmed reaction (TPR), XRD, and Raman spectroscopy as well as gravimetrical analysis employing an on-line microbalance coupled with a mass spectrometer (MS) confirm that the redox properties can be tuned by varying the

(1) Khlobystov, A. N.; Britz, D. A.; Briggs, G. A. D. *Acc. Chem. Res.* **2005**, *38*, 901.
(2) Santiso, E. E.; George, A. M.; Sliwinska-Bartkowiak, M.; Nardelli, M. B.; Gubbins, K. *Adsorption* **2005**, *11*, 349.
(3) Halls, M. D.; Schlegel, H. B. *J. Phys. Chem. B* **2002**, *106*, 1921.
(4) Ajayan, P. M. *Chem. Rev.* **1999**, *99*, 1787.
(5) Planeix, J. M.; Coustel, N.; Coq, B.; Bretons, V.; Kumbhar, P. S.; Dutartre, R.; Geneste P.; Bernier P.; Ajayan P. M. *J. Am. Chem. Soc.* **1994**, *116*, 7935.
(6) Serp, P.; Corrias, M.; Kalck, P. *Appl. Catal. A* **2003**, *253*, 337.
(7) Yoon, B.; Wai, C. M. *J. Am. Chem. Soc.* **2005**, *127*, 17174.
(8) Girishkumar, G.; Hall, T. D.; Vinodgopal, K.; Kamat, P. V. *J. Phys. Chem. B* **2006**, *110*, 107.
(9) Tessonnier, J.; Pesant, L.; Ehret, G.; Ledoux, M. J.; Pham-Huu, C. *Appl. Catal. A* **2005**, *288*, 203.
(10) Zhang, A. M.; Dong, J. L.; Xu, Q. H.; Rhee, H. K.; Li, X. L. *Catal. Today* **2004**, *93−95*, 347.
(11) Ajayan, P. M.; Ebbesen, T. W.; Ichihashi, T.; Iijima, S.; Tanigaki, K.; Hiura, H. *Nature* **1993**, *362*, 522.
(12) Guerret-Plecourt, C.; Le Bouar, Y.; Lolseau, A.; Pascard, H. *Nature* **1994**, *372*, 761.
(13) Chen, Y. K.; Chu, A.; Cook, J.; Green, M. L. H.; Harris, P. J. F.; Heesom, R.; Humphries, M.; Sloan, J.; Tsang, S. C.; Turner, J. F. C. *J. Mater. Chem.* **1997**, *7*, 545.
(14) Westerberg, S.; Wang, C.; Chou, K.; Somorjai, G. A. *J. Phys. Chem. B* **2004**, *108*, 6374.
(15) Weiss, W.; Zscherpel, D.; Schloegl, R. *Catal. Lett.* **1998**, *52*, 15.
(16) Chen, W.; Pan, X.; Willinger, M. G.; Su, D. S.; Bao, X. *J. Am. Chem. Soc.* **2006**, *128*, 3136.

nature of the host (CNTs, SBA-15), the location on the exterior or interior surface of CNTs, and the diameter of the CNT channels. In particular Raman spectra indicate that the Fe−O vibration modes of the encapsulates are sensitive to the inner diameter of CNTs.

2. Experimental Section

2.1. Material Synthesis. Raw CNTs (Chengdu Organic Chemicals) were first treated in aqueous HNO_3 solution following a procedure adapted from the literature.[17] Briefly, 3 g of CNTs were suspended in 150 mL of concentrated HNO_3 (68 wt %) and refluxed at 140 °C in an oil bath. Our experiments with different refluxing durations (3−20 h) indicated that almost all CNTs had opened tips after refluxing for 14 h. After the mixture was cooled down to room temperature, it was filtered through a PTFE film with a pore diameter of 0.2 μm and washed with deionized water until the pH value of the filtrate was around 7. Then the product was dried at 60 °C for 12 h. This treatment removes the caps of the nanotubes as well as amorphous carbon and metal catalyst residues. The treated nanotubes were subsequently added into an aqueous $Fe(NO_3)_3$ solution under stirring followed by ultrasonic treatment and simultaneous stirring for 2 h. Then the solvent was evaporated slowly under ambient conditions. The resulting solid mixture was gradually heated to 140 °C in air and kept for 8 h at this temperature before being heated to 350 °C in He at a rate of 2 °C/min and held there for 3 h. In this way, $Fe(NO_3)_3$ decomposes inside CNTs into Fe_2O_3 and the obtained sample is denoted as Fe_2O_3-*in*-CNT(x). The x in parentheses represents the smallest inner diameter of a CNT type. Three types of CNTs are used: CNT(2) (i.d. 2−5 nm), CNT(4) (i.d. 4−8 nm), and CNT(8) (i.d. 8−12 nm). The loading of Fe_2O_3 is 8 wt % for all samples unless otherwise stated. TEM reveals that 80 ± 5% particles are located inside the nanotube channels of the Fe_2O_3-*in*-CNT(x) samples, while the rest resides on the outer surface of CNTs (vide infra).

For comparison, the same amount of Fe_2O_3 was deposited on the outer surface of nanotubes by impregnating CNT(4) with aqueous $Fe(NO_3)_3$ solution. For this CNT(4) with closed caps were used, which were obtained by refluxing CNTs in 37 wt % HNO_3 solution at 110 °C for 5 h. In the TEM images of these CNTs, we did not observe tubes with opened caps. After impregnation, the same drying procedure was applied and Fe_2O_3-*out*-CNT(4) was obtained.

Fe-*in*-CNT(4) and Fe-*out*-CNT(4) were obtained by reduction of Fe_2O_3-*in*-CNT(4) and Fe_2O_3-*out*-CNT(4) with Fe_2O_3 loading of 20 wt % in flowing H_2 at 500 °C, respectively.

2.2. Characterization. Transmission electron microscopy (TEM) measurements were carried out on a FEI Tecnai G^2 microscope operated at an accelerating voltage of 120 kv. The samples were ultrasonically suspended in ethanol and placed onto a carbon film supported over a copper grid.

The optical spectrum of the blank CNT sample indicates a maximum absorption in the UV−vis range peaking at about 255 nm (see Supporting Information, Figure S1). Therefore, we chose the He−Ne laser with an excitation wavelength of 632.8 nm for characterization of the Fe_2O_3 encapsulated within CNTs, because longer wavelength light is expected to penetrate deeper into the sample.[18−19] Raman experiments were carried out on a LabRam I confocal microprobe Raman instrument (Dilor, France) at a laser power of ca. 7 mW. The powdered sample was pressed into the sample holder, which was then placed into a home-built high-temperature reaction cell for in situ Raman measurements.[20]

For monitoring the autoreduction temperature of an Fe_2O_3 encapsulate by Raman spectroscopy, a sample was heated in Ar at a rate of 2 °C/min up to 500 °C and then cooled down to around 30 °C. Subsequently, a Raman spectrum was recorded. Then this heating, cooling, and recording procedure was repeated increasing the maximum temperature during these cycles in 10 °C steps until 650 °C (upper temperature limit of the in situ cell). In this way the dependence of the Fe_2O_3 autoreduction temperature on the CNT diameter was probed. This autoreduction process was also followed by mass spectrometry by heating the samples in a flowing He stream (30 mL/min) at a rate of 2 °C/min. Since the reduction of Fe_2O_3 by carbon yields CO as the main product, the CO signal (m/e = 28.06) was monitored by an online quadrupole mass spectrometer (MS, Balzers OmniStar 300). In addition, the chemical transformation from Fe_2O_3 to metallic Fe of the samples was followed by in situ XRD (Rigaku X-ray diffractometer). Diffraction patterns were recorded within a 2θ range of 30°−50° continuously while the samples were heated at a rate of 2 °C/min since the most intense diffraction peaks of Fe and Fe_2O_3 phases are located in this 2θ range. The scanning speed was 10°/min.

The oxidation behavior of Fe nanoparticles was studied in situ XRD by heating the samples in a gas mixture of O_2/He (1 vol %) at a rate of 2 °C/min. The samples Fe-*in*-CNT(4) and Fe-*out*-CNT(4) had been obtained by prereduction of the oxides in the in situ XRD cell. Following reduction the cell was purged by a He stream for 30 min to remove residual H_2 prior to oxidation. The diffraction patterns were again recorded within 2θ = 30°−50° during the reoxidation process.

The oxidation process was also investigated by gravimetrical analysis employing a microbalance (TEOM, Rupprecht & Patashnick). Simultaneously the composition of the effluents was analyzed by an online MS. This TEOM operates with fixed-bed samples with reaction gases passing through the catalyst bed and allows a highly accurate measurement of the mass change (Δm = 10 μg) at a high time resolution (Δt = 0.1 s).

3. Results and Discussion

3.1. Morphology of the Fe_2O_3/CNT Composites. TEM images reveal that the Fe_2O_3 particles of Fe_2O_3-*out*-CNT(4) are homogeneously dispersed on the outer surface of the nanotubes. The particle size is fairly uniform with over 80% particles having a size in the range of 5−8 nm. In the samples of Fe_2O_3-*in*-CNT(x), we found that there are 80 ± 5% particles located inside the tubes (Table S1). Figure 1 shows TEM images of these samples and the corresponding size distributions of overall particles. It can be seen that the particle size of Fe_2O_3 varies with the diameter of CNTs. It is around 6−8 nm in CNT(8), 5−7 nm in CNT(4), and 3−4 nm in CNT(2), respectively. Note that the outside particles are of a very similar size as those inside the tubes in the respective sample.

3.2. Raman Spectroscopic Study of the Encapsulated Fe_2O_3 Particles. The spectrum of the blank CNT(4) sample exhibits two Raman bands centered around 1590 and 1325 cm^{-1}, which correspond to the characteristic E_{2g} and D modes of carbon nanotubes, respectively.[21−22] We do not observe Raman bands from CNT(4) in the frequency region below 1000 cm^{-1} and in particular the 200−600 cm^{-1} range where the characteristic Fe−O vibration bands of iron oxides are located,[23] as shown in Figure 2A-a. After deposition of Fe_2O_3 particles on the outer surface of CNT(4) three new Raman bands appear at 215, 273, and 383 cm^{-1} (Figure 2A-b), respectively. These bands are in agreement with the typical frequencies observed

(17) Tsang, S. C.; Chen, Y. K.; Harris, P. J. F.; Green, M. L. H. *Nature* **1994**, *372*, 159.
(18) Dombrowski, K. F.; De Wolf, I.; Dietrich, B. *Appl. Phys. Lett.* **1999**, *75*, 2450.
(19) Holtz, M.; Duncan, W. M.; Zollner, S.; Liu, R. *J. Appl. Phys.* **2004**, *88*, 2523.
(20) Weng, W.; Pei, X.; Li, J.; Luo, C.; Liu, Y.; Lin, H.; Huang, C.; Wan, H. *Catal. Today* **2006**, *117*, 53.
(21) Wang, Y.; Alsmeyer, D. C.; McCreery, R. L. *Chem. Mater* **1990**, *2*, 557.
(22) Ekund, P. C.; Holden, J. M.; Jishi, R. A. *Carbon* **1995**, *33*, 959.
(23) De Faria, D. L. A.; Silva, S. V.; De Oliveira, M. T. *J. Raman Spectrosc.* **1997**, *28*, 873.

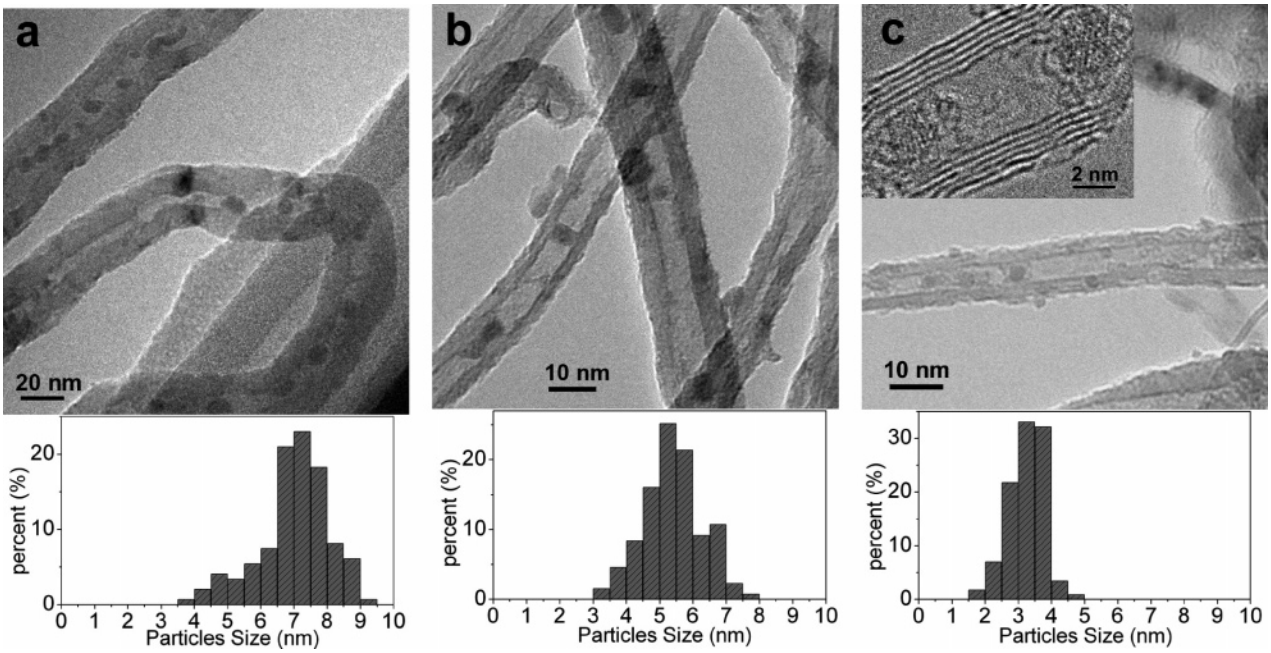

Figure 1. TEM images and the size distributions of the Fe_2O_3 nanoparticles encapsulated within CNTs with varying inner diameters (a) CNT(8) with i.d. 8−12 nm; (b) CNT(4) with i.d. 4−8 nm; (c) CNT(2) with i.d. 2−5 nm.

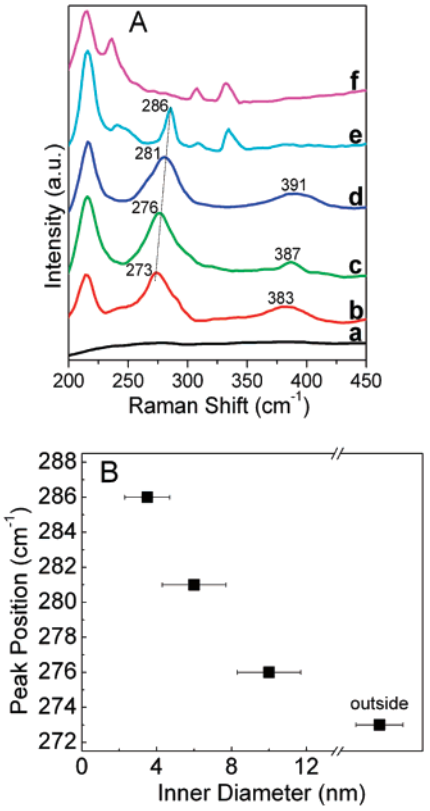

Figure 2. (A) Room-temperature Raman spectra of the Fe_2O_3 particles encapsulated within various CNT channels. (a) Blank CNT(4); (b) Fe_2O_3-*out*-CNT(4); (c) Fe_2O_3-*in*-CNT(8); (d) Fe_2O_3-*in*-CNT(4); (e) Fe_2O_3-*in*-CNT-(2); (f) blank CNT(2). (B) Raman shift versus the inner diameter of CNTs.

for α-Fe_2O_3, although a shift toward lower frequency is noted compared to the reported features for the bulk material (220, 283, and 396 cm^{-1}).[23] These features can be assigned to the A_{1g} (215 cm^{-1}) and E_g (273 and 383 cm^{-1}) vibration modes of Fe−O.[23] Since the feature at 215 cm^{-1} is too close to the side band of the excitation laser line, we do not pay detailed attention to this band in the following.

When Fe_2O_3 particles are introduced inside the channels of CNT(8), there also appear three new bands with the latter two centered at 276 and 387 cm^{-1} (Figure 2A-c). They are blue-shifted compared to those for the Fe_2O_3 particles on the outer surface of CNT(4). Figure 2A-d shows that these two bands further shift to 281 and 391 cm^{-1} inside CNT(4), respectively. Note that there is an 8 cm^{-1} shift of each Fe−O mode between exterior and interior Fe_2O_3 particles of CNT(4). The first E_g mode is further blue-shifted to 286 cm^{-1} in the spectrum of Fe_2O_3-*in*-CNT(2), while the second one is hardly discernible as a very broad and weak band between 390 and 400 cm^{-1} there (Figure 2A-e and the inset of Figure S2). In addition this sample exhibits a few new features at 214, 235, 307, and 331 cm^{-1}, which can be assigned to modes of SWNTs by comparison with the spectrum of the blank CNT(2) (Figure 2A-f).[24]

It should be pointed out that the metal−O vibrations could be influenced by the particle size due to an increased fraction of surface atoms, confinement of optical phonons, crystal defects, and etc.[25−26] Figure 2B shows the Raman shift of the more intense E_g Fe−O band versus the inner diameter of CNT-(*x*), in which the particle size of Fe_2O_3 varies accordingly. One sees that this ν_{Fe-O} frequency of Fe_2O_3 nanoparticles on Fe_2O_3-*out*-CNT(4) is significantly red-shifted compared to the bulk Fe_2O_3 in agreement with the general observation in earlier reports.[23,27−29] However, it shifts to higher frequencies when the particles are moved from the exterior to the interior of CNTs. It further blue-shifts when the particle size becomes smaller inside narrower CNT channels. This does not line up with the

(24) Dresselhaus, M. S.; Dresselhaus, G.; Jorio, A.; Souaz Filho, A. G.; Saito, R. *Carbon* **2002**, *40*, 2043.
(25) Xu, J. F.; Ji, W.; Shen, Z. X.; Li, W. S.; Tang, S. H.; Ye, X. R.; Jia, D. Z.; Xin, X. Q. *J. Raman Spectrosc.* **1999**, *30*, 413.
(26) Liu, F. X.; Yang, J. L.; Zhao, T. P. *Phys. Rev. B* **1997**, *55*, 8847.
(27) Owens, F. J.; Orosz, J. *Solid State Commun.* **2006**, *138*, 95.
(28) Wang, X.; Chen, X. Y.; Ma, X. C.; Zheng, H. G.; Ji, M. R.; Zhang, Z. D. *Chem. Phys. Lett.* **2004**, *384*, 391.
(29) Wang, J.; White, W. B.; Adair, J. H. *J. Am. Ceram. Soc.* **2005**, *88*, 3449.

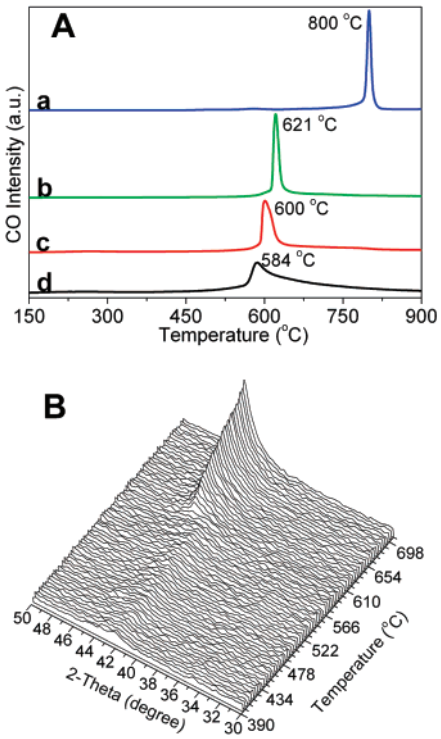

Figure 3. (A) CO evolution during TPR of the Fe_2O_3/CNT composites. (a) Fe_2O_3-*out*-CNT(4); (b) Fe_2O_3-*in*-CNT(8); (c) Fe_2O_3-*in*-CNT(4); (d) Fe_2O_3-*in*-CNT(2). (B) the chemical transformation of Fe_2O_3-*in*-CNT(2) monitored by in situ XRD.

red shift generally reported for nanosized Fe_2O_3[23,27−29] implying the presence of an interaction of the Fe_2O_3 particles with the inner CNT surface. Furthermore, this interaction is enhanced within smaller nanotubes.

Raman spectroscopy has been widely used to study transition metal oxides and is also a proven method to characterize graphitic carbon including CNTs.[21−29] The above results demonstrate that this technique is also effective for the investigation of the encapsulated transition metal oxide particles. Furthermore, it is a powerful tool to probe the differences in the interaction of the encapsulated and surface nanoparticles with CNTs. To the best of our knowledge, this is the first example of employing Raman spectroscopy for this purpose opening a new avenue for the notoriously difficult study of encapsulates in CNTs.

3.3. Autoreduction of the Encapsulated Fe_2O_3 Particles. The interaction of the Fe_2O_3 nanoparticles with the inner and outer CNT surfaces affects the autoreduction behavior of Fe_2O_3.[16] This interaction was studied in greater detail here by temperature programmed reaction (TPR) focusing on the influence of the CNT inner diameter. The evolution of CO was monitored in the effluent while heating the samples in a He stream. Figure 3A-a shows that the Fe_2O_3 particles located on the outer surface of CNT(4) are reduced at 800 °C. When the Fe_2O_3 particles are moved into the interior of CNT(8), the reduction takes place at 621 °C (Figure 3A-b). With the diameter decreasing, the reduction temperature is stepwise lowered to 600 °C (CNT(4), Figure 3A-c) and further down to 584 °C if the Fe_2O_3 particles are located inside CNT(2) (Figure 3A-a). The area of the CO peak of each sample in Figure 3A is practically the same. However, the peak becomes wider and asymmetric with decreasing diameter, which is caused by the increasingly difficult diffusion of CO out of the nanotubes as indicated by a reduction experiment with Fe_2O_3-*in*-CNT(2) at a heating rate of 0.5 °C/min.

Table 1. Autoreduction Temperatures (*T*) of the Encapsulated Fe_2O_3 within Various CNTs Detected by TPR, in situ XRD, and Raman Spectroscopy

sample	*T* by TPR (°C)	*T* by XRD (°C)	*T* by Raman (°C)
Fe_2O_3-*in*-CNT(8)	621	∼ 615	∼ 620
Fe_2O_3-*in*-CNT(4)	600	∼ 600	∼ 610
Fe_2O_3-*in*-CNT(2)	584	∼ 590	∼ 590

In situ XRD detects the crystal phase changes of the samples accurately without interference by the CO diffusion. The XRD patterns in Figure 3B show the transformation of the encapsulated Fe_2O_3-*in*-CNT(4) during the heating in Ar. The two weak peaks at 34.5° and 42.6° are the characteristic [110] and [202] diffraction peaks of Fe_2O_3 (JCPDS 24-0072). The latter peak overlaps with the [100] diffraction peak of graphite (JCPDS 65-6212). The two Fe_2O_3 peaks do not change significantly between room temperature and 585 °C. However in a narrow range of 590 ± (1−5) °C, the Fe_2O_3 phase vanishes abruptly, while a new peak rises at 44.1° corresponding to the [110] reflection of the metallic Fe phase (JCPDS 06-0696). This is in very good accordance with the reduction temperature detected by the CO release during TPR. The 44.1° peak becomes more intense with a further increase in temperature. The disappearance of Fe_2O_3 and appearance of Fe phases are also observed for the other samples within a narrow temperature range. The XRD transformation temperatures of these samples also agree well with those corresponding to the maximum intensity of the respective CO MS signals detected by TPR, as shown in Table 1. This implies that the CO diffusion does not delay the detection of the reduction temperature by TPR significantly.

The autoreduction was further studied in situ by tracking the characteristic Fe−O Raman band. As shown in Table 1 (also see Figure S3), the band 276 cm^{-1} of Fe_2O_3-*in*-CNT(8) disappears at ∼ 620 °C indicating that the oxide has been reduced to metallic Fe because metals are not Raman active. The 281 cm^{-1} ν_{Fe-O} mode inside CNT(4) becomes very weak near 600 °C and vanishes at ∼610 °C, and the corresponding 286 cm^{-1} feature within CNT(2) disappears at ∼590 °C. These temperatures agree well with those observed by TPR and in situ XRD. This further corroborates that we can monitor Fe_2O_3 nanoparticles inside CNTs by Raman spectroscopy. In summary these experiments demonstrate conclusively that the autoreduction of the encapsulated Fe_2O_3 nanoparticles varies with the inner diameter of CNTs and is significantly facilitated within smaller CNT channels.

We have previously proposed that an electron deficiency of the interior CNT surface is responsible for the facilitated autoreduction of the encapsulated Fe_2O_3.[16] Deviation from planarity causes hybridization to become intermediate between sp^2 and sp^3 in the graphene layers, and as a result π-electron density is shifted from the concave inner to the convex outer surface of CNTs.[30−31] Thus the interior surface becomes electron-deficient while the outer surface becomes electron-enriched. Probably this electron density loss can be at least

(30) Haddon, R. C. *Science* **1993**, *261*, 1545.
(31) Ugarte, D.; Chatelain, A.; de Heer, W. A. *Science* **1996**, *274*, 1897.

partially compensated through interaction with the encapsulated Fe_2O_3. Apparently this destabilizes the oxidic nanoparticles and facilitates the autoreduction of the encapsulates. This electron shift should be enhanced as the CNT cross section becomes smaller and should result in a stronger electronic interaction of the concave inner surface with the encapsulated Fe_2O_3 particles. The clear correlation of the autoreduction temperature with the CNT inner diameter observed here is consistent with this initial hypothesis of us.

3.4. Oxidation of the Encapsulated Fe Nanoparticles. The oxidation of the Fe nanoparticles inside and outside CNT(4)s with 1% O_2 in He is studied by in situ XRD. As shown in Figure 4, both the fresh Fe-*out*-CNT(4) and Fe-*in*-CNT(4) exhibit an intense peak at $2\theta = 44.1°$ and a much weaker one at 42.7°. The former peak corresponds to the characteristic metallic Fe [110] reflection, and the latter, to graphite [100]. Figure 4A shows that the intensity of the Fe phase on Fe-*out*-CNT(4) starts to decrease at ~90 °C (denoted as T_1), while at ~105 °C (T_2) the [110] Fe_2O_3 peak at $2\theta = 34.5°$ starts to emerge. The latter peak grows more intense with increasing temperature, and around 250 °C other peaks at 32.4, 40.1 and 48.6° are also observed corresponding to the [104], [113], and [024] Fe_2O_3 facets, respectively. The metal peak at 44.1° vanishes around 290 °C (T_3) suggesting that the oxidation of Fe is completed.

In contrast, the significant decline of the Fe is observed at ~160 °C (T_1), and the emergence of the Fe_2O_3 phase only starts to be discernible at 180 °C (T_2) on Fe-*in*-CNT(4) and the Fe phase does not fully disappear until 405 °C (T_3) (Figure 4B), almost 100 °C higher than the case for Fe-*out*-CNT(4). The key temperatures (T_1, T_2, and T_3) of both samples are listed in Table 2 for comparison. The plot in Figure 4C shows the intensity of the metallic Fe phases changing with the oxidation temperature, from which the Fe oxidation rate can be roughly approximated. Thus the activation energy was estimated to be 18 kJ/mol for the oxidation of the encapsulated Fe nanoparticles of Fe-*in*-CNT(4), which is higher than the corresponding value of 14 kJ/mol for Fe-*out*-CNT(4). Both values are much smaller than the 32 kJ/mol reported for the oxidation of bulk Fe.[32] This clearly indicates that nanosized Fe particles are more readily oxidized, even though the encapsulated Fe is more difficult to oxidize.

In an independent experiment the oxidation process is monitored by following the mass change of the samples and the composition of the effluent. The results are shown in Figure 5, in which dashed lines represent Fe-*out*-CNT(4) and solid lines represent Fe-*in*-CNT(4). One sees that the mass of Fe-*out*-CNT-(4) starts to increase at ~100 °C and reaches a plateau at ~320 °C. In parallel the O_2 signal decreases to a minimum at ~250 °C (Figure S4) indicating that the oxidation of the Fe nanoparticles is completed in that temperature range. This is consistent with a temperature of 290 °C where the XRD diffraction of the metallic Fe phase completely disappears (Table 2). Note that the oxidation of Fe loaded on activated carbon (Vulcan XC-72) is found to start and finish at temperatures similar to those detected for Fe-*out*-CNT(4). Figures 5 and S4 also show that above 320 °C the O_2 consumption increases again concomitant with the evolution of CO_2 due to the oxidation of CNTs.

(32) Grosvenor, A. P.; Kobe, B. A.; McIntyre, N. S. *Surf. Sci.* **2005**, *574*, 317.

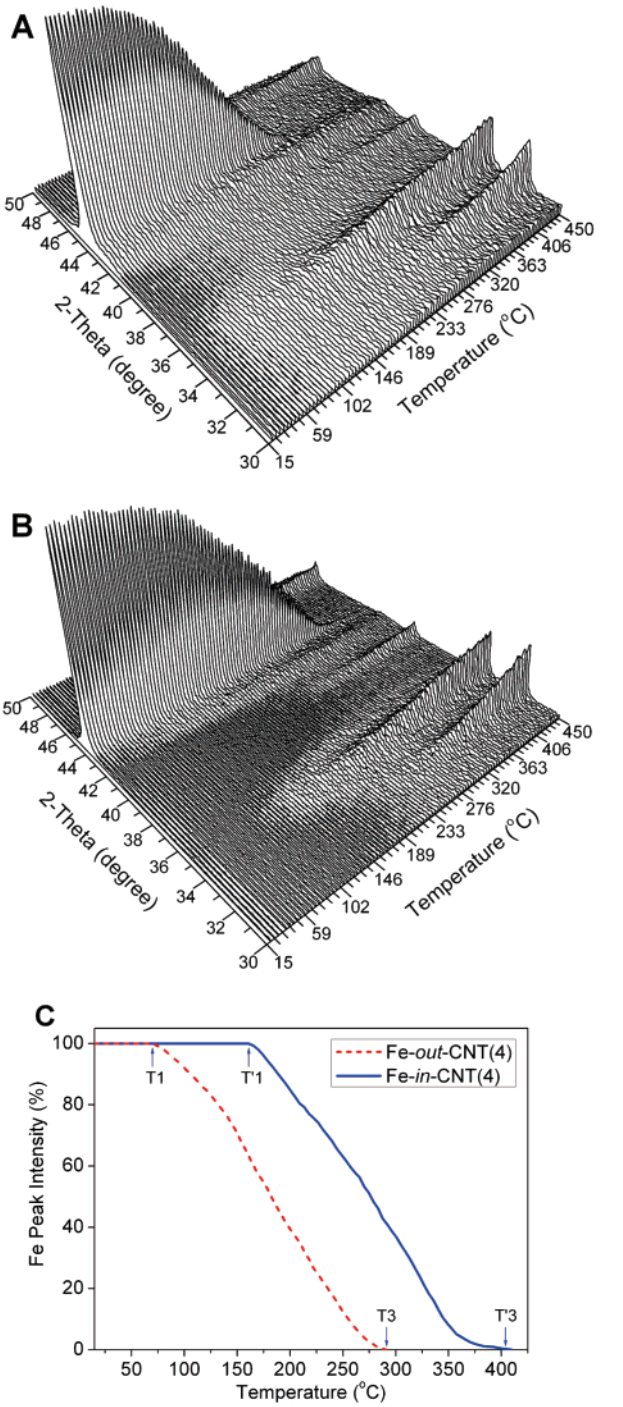

Figure 4. In situ XRD patterns of (A) Fe-*out*-CNT(4); (B) Fe-*in*-CNT(4); (C) the intensity change of the Fe diffraction peaks during temperature programmed oxidation. The dotted line in (C) denotes Fe-*out*-CNT(4), and the solid line, Fe-*in*-CNT(4).

The solid line in Figure 5 shows that the sample mass of Fe-*in*-CNT(4) increases only above 150 °C significantly and passes through a narrow plateau at ~430 °C, while the O_2 signal reaches a minimum at ~365 °C (Figure S4). This agrees again very well with the in situ XRD measurements (Table 2). These temperatures are higher than the corresponding ones for Fe-*out*-CNT(4). Interestingly, the oxidation of CNTs and the concomitant CO_2 release of Fe-*in*-CNT(4) are also shifted by approximately 50 °C to higher temperatures. This suggests that the Fe_2O_3 nanoparticles catalyze the oxidation of CNTs.

Table 2. Oxidation Temperatures Detected by in Situ XRD and Gravimetrical Method Using an Online Microbalance[a]

	in situ XRD			mass change	
sample	T_1 (°C)	T_2 (°C)	T_3 (°C)	T_4 (°C)	T_5 (°C)
Fe-*out*-CNT(4)	90	105	290	100	320
Fe-*in*-CNT(4)	160	180	405	150	430

[a] T_1: the temperature when the intensity of the Fe diffraction peak starts to decrease. T_2: the temperature when the Fe_2O_3 peak emerges. T_3: when the diffraction peak of metallic Fe disappears. T_4: when the sample mass starts to increase due to oxidation. T_5: when the sample mass reaches a plateau.

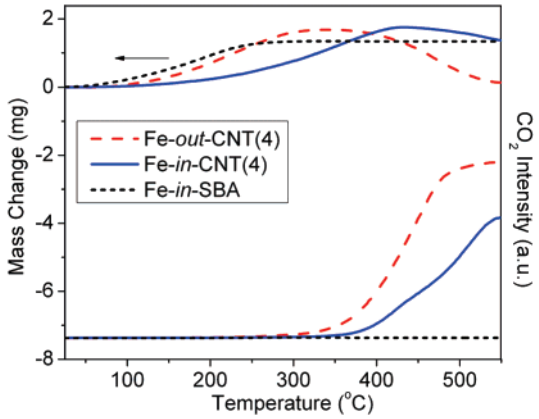

Figure 5. Change of the sample mass and the effluent composition during temperature programmed oxidation. Dashed line represents Fe-*out*-CNT-(4); solid line represents Fe-*in*-CNT(4); dotted line represents Fe-*in*-SBA encapsulates.

The oxidation of the encapsulated Fe particles requires oxygen to diffuse into CNT channels. In order to evaluate the influence of diffusion inside nanotubes we deposited Fe particles within SBA-15 channels (Fe-*in*-SBA). SBA-15 is a mesoporous silica exhibiting a similar morphology with respect to the channel length (300−600 nm) and inner diameter (6−7 nm) as CNT-(4). Thus these channels can provide a similar geometrical confinement for the Fe particles and similar diffusion path for oxygen to the Fe. The dotted line in Figure 5 shows that the mass of the sample Fe-*in*-SBA begins to increase above 50 °C and it levels off around 260 °C. In addition, no obvious change of the O_2 signal (Figure S4) is observed with further increasing temperature, suggesting that the oxidation has been completed. This temperature is even lower than that for Fe-*out*-CNT(4). Therefore the oxygen diffusion due to mere geometrical constriction is not slowing down the oxidation of the encapsulated Fe particles. Instead, it appears to be the interaction with the inner CNT surface that has delayed the oxidation of the Fe nanoparticles.

There is a vast body of work devoted to the electronic interaction between transition metals and graphene sheets in both graphite and CNTs. However, those studies focus almost exclusively on the magnetic properties of the transition metals, but next to nothing is said about their redox properties. Nevertheless, some implications for the redox behavior of the transition metals can be inferred. Studies show that the p_z orbitals of graphitic carbon (π-bonded states) hybridizes strongly with the d orbitals of transition metals such as Fe.[33−34] This hybridization leads to a small electron transfer to the graphite,[35] which impedes the oxidation of the transition metal and could explain the slightly higher oxidation temperature of Fe-*out*-CNT-(4) compared to Fe-*in*-SBA. Furthermore, because of the curvature of the graphene sheets in CNTs the corresponding coordination of the transition metal atoms differs between the concave inside and the convex outside of the nanotubes.[33] It has been pointed out above that the interior CNT surface is electron deficient with respect to the planar graphite surface.[30−31] Thus, it can be assumed that the electron transfer from Fe to the interior CNT surface is enhanced with respect to the outer surface. Consequently, the oxidation of the encapsulated Fe should be more strongly retarded just as we have observed here.

4. Conclusions

The redox behavior of iron and iron oxide nanoparticles encapsulated within CNTs has been studied in detail. Raman spectroscopy was employed for the first time to investigate such encapsulates. The spectra reveal that characteristic Fe−O modes are red-shifted in the nanoparticles in comparison to bulk Fe_2O_3. However, this frequency shift is reversed when the Fe_2O_3 particles are moved inside the CNT channels. A further blue shift is observed with a decreasing inner diameter, suggesting an interaction of the nanoparticles with the inner CNT surface. As a consequence the reduction of Fe_2O_3 nanoparticles is facilitated and depends on the diameters of CNT channels, as conclusively evidenced by temperature programmed reaction, in situ XRD, and Raman spectroscopy. The chemical transformation during reoxidation of the Fe particles was monitored by in situ XRD and online gravimetrical analysis, indicating that the Fe oxidation is also sensitive to the support and the dimensions of the channels. We found that the oxidation temperature increases in the following sequence: inside SBA-15 channels < on XC-72 ≈ on outer surface of CNTs < inside CNT channels. Obviously, the reactivity of the oxidic Fe particles is increased while that of the metallic counterparts is decreased inside CNTs. This is attributed to an electron transfer between the Fe encapsulates and the CNT graphene sheets, which in effect stabilizes the metallic state of Fe. However, this tuning of the redox behavior of transition metal nanoparticles within CNTs is currently not well understood from a fundamental point of view. Therefore, further experimental and theoretical studies on the redox properties of these novel and very promising composite catalysts are highly desirable.

Acknowledgment. We thank Prof. Zhongqun Tian, Prof. Weizheng Weng, and Ms. Jianmei Li from Xiamen University (China) for providing convenience for Raman spectroscopy experiments; Mr. Songhua Yu for the assistance during the XRD measurements; and Dr. Andreas Goldbach for discussions. This work was supported by grants from the National Natural Science Foundation of China (Project No. 20503033, 90206036, and 20573107).

Supporting Information Available: The UV−vis spectrum of CNT(4), in situ Raman spectra of samples Fe_2O_3-*in*-CNT-(*x*), and mass change of samples during oxidation. This material is available free of charge via the Internet at http://pubs.acs.org.

JA0713072

(33) Yagi, Y.; Briere, T. M.; Sluiter, M. H.; Kumar, V.; Farajian, A. A.; Kawazoe, Y. *Phys. Rev. B* **2004**, *69*, 075414.
(34) Meon, M.; Andriotis, A. N.; Froudakis, G. E. *Chem. Phys. Lett.* **2000**, *320*, 425.
(35) Duffy, D. M.; Blackman, J. A. *Phys. Rev. B* **1998**, *58*, 7443.